ICAS 2016
30th Congress of the International Council of the Aeronautical Sciences
DCC, Daejeon, Korea ; September 25-30, 2016

STUDY ON EFFICIENT FULL ANNULUS URANS COMPUTATIONS OF AN INTAKE COMPRESSOR CONFIGURATION

Thomas Kächele*, Tim Schneider, and Reinhard Niehuis***
***Universität der Bundeswehr München, ****MTU Aero Engines AG**

Keywords: *transonic compressor, s-duct, inflow distortion, full annulus simulations*

Abstract

Modern complex intake geometries generate combined total pressure and swirl distortions towards the compression system of jet engines. In the current intake design workflow, duct geometries are assessed experimentally or numerically as a separated unit and evaluated by distortion parameters. These are then compared to the stability limits within engine specification. This approach neglects the influence of the (distorted) compressor on the intake flow. To understand these interactions, coupled simulations of the intake and the full annulus of a transonic three stage compressor are carried out. In advance, sensitivity studies of the spatial and temporal discretization are undertaken, in order to reduce the high computational effort as well as to quantify the resulting deficits in precision. In the first part, an initial mesh density, based on experience gained on previous projects, is coarsened and evaluated on the basis of steady passage calculations. A significant reduction of cell numbers could be achieved through a combination of coarsening within the passage and a reduction of the blade wall distances. The subsequent time-step study starts with the definition of suited convergence criteria for unsteady calculations. Afterwards the influences of a coarsened time-step on compressor and stage characteristics as well as on the unsteady rotor-stator interactions are presented. As the demands on the later flow field analysis of the coupled setup are reduced to machine and stage characteristics, a reduction of the commonly used temporal resolution by a factor of two is still valid for the present setup. The unsteady simulation of the intake flow field requires several rotor revolutions to develop its low frequency unsteady behavior. This setup comprises of about 102 million cells and a simulated time of more than 15 rotor revolutions until a kind of periodic state is achieved. On the available 128 computing cores about 35 days of calculation time arise for the simulation of one engine operation point. The results will later be validated by experimental data, which is expected to be generated by mid 2016.

Nomenclature

Symbols

DC60	total pressure distortion coefficient
Δ	difference
f	frequency
p_t	total pressure
Π_t	total pressure ratio
q	flow variable
SC60	swirl distortion coefficient
θ	circumferential angle
y^+	non dimensional wall distance

Subscripts

max	maximum
norm	normalized value
ref	reference
R1	rotor 1

Abbreviations

AIP	Aerodynamic Interface Plane
BPF	Blade Passing Frequency
ETF	Engine Test Facility
FFT	Fast Fourier Transformation
LPC	Low Pressure Compressor

1 Introduction

The evolution of aircraft design leads to more and more integrated propulsion systems. While

civil blended or hybrid wing body concepts aim on a higher aircraft fuel efficiency by e.g. boundary layer ingestion, a low observability using bent intake ducts lies in the focus of military applications. These complex intake geometries generate combined total pressure and swirl distortions towards the compression system of jet engines. A lower performance and a reduction of stability margin are the consequences [1]. Commonly, intake and engine are regarded as separate units delivered by the cell and the engine manufacturer, respectively. Therefore, isolated duct geometries are assessed experimentally or numerically [2] to evaluate the resulting distortion patterns within the Aerodynamic Interface Plane (AIP) between intake and fan stage as shown in Fig. 1.

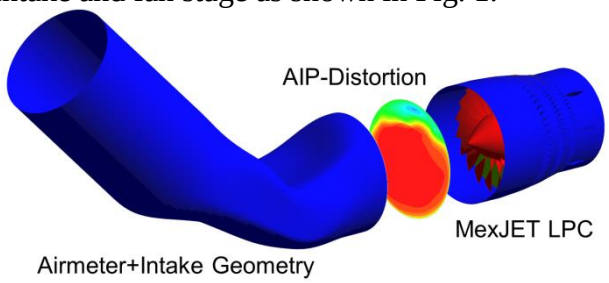

Fig. 1. Intake geometry, AIP-distortion and compressor

These patterns are then evaluated in terms of distortion parameters and compared to the stability limits within engine specification based on experimental investigations by the engine manufacturer. This approach neglects two facts:

First, the conventional distortion parameters such as DC60 or SC60 [3] only give a rudimentary representation of the rather complex distortion patterns generated by bent intake geometries. Second, the compressor itself influences the intake flow distortion in upstream direction through pressure signals produced by e.g. shock waves. Thus, the AIP flow conditions calculated for isolated duct geometries are different to the ones actually experienced by the compressor.

Up to date highly resolved numerical simulations of distorted compression systems have only been carried out with generic distortion patterns in research projects due to the high computational costs [4],[5]. The comparison with exhaustive available experimental data shows that numerical simulations based on unsteady Reynolds averaged Navier-Stokes (URANS) equations are capable of predicting the dominant flow phenomena of distorted compressors.

Within the scope of a current research project at the Institute of Jet Propulsion of the University of the German Federal Armed Forces Munich in cooperation with MTU Aero Engines AG, experimental investigations of a full size intake in combination with the institute's MexJET engine are in preparation [6].

In parallel, URANS simulations of the intake and the transonic three-stage low-pressure compressor (LPC, cf. Fig. 1) are carried out. These simulations focus on the interactions of the intake flow distortion and the compressor as well as the upstream influence of the compressor on the duct flow. Concerning the compression system, validation data will only be available at the inlet and outlet of the LPC. Thus, the commonly used temporal and spatial resolution, related with high computational effort needs to be reduced to allow a simulation of all three compressor stages.

2 Numerical Setup

2.1 Flow Solver

For the present calculations, the flow solver TRACE [7],[8] is used. This 3D finite volume code is developed by the DLR-AT and MTU Aero Engines AG and was already validated for full annulus calculation of distorted low pressure compressors [9],[10]. It solves the discretized (U)RANS equations on structured multi-block meshes. Fully turbulent mode was used due to Reynolds numbers of $5.25 \cdot 10^6$ and $2.52 \cdot 10^6$ based on intake diameter and fan blade chord respectively. Turbulence is modelled by the Wilcox k-ω model with an additional correction for rotational effects proposed by Bardina and a stagnation point anomaly fix according to Kato-Launder [11].

2.2 Available Resources

The calculation resources of the project limit the degree of detail that could be achieved by the

coupled simulations. 128 cores were available with a maximum RAM of 512GB. In order to accomplish good parallelization efficiency, the maximum number of mesh cells per CPU should be not higher than 0.6m. Therefore, a mesh size of about 80m cells was initially aimed for.

2.3 Normalization and Averaging

In the context of this paper, most values are normalized by a defined reference value q_{ref}.

$$q_{norm} = \frac{q}{q_{ref}} \quad (1)$$

In the case of normalized differences, the following formulation is used

$$\Delta q_{norm} = \frac{(q - q_{ref})}{q_{ref}} \quad (2)$$

A simple arithmetic averaging is used for temporal averages. Spatial averages of flux variables are flux averaged.

3 Isolated LPC Simulations

The MexJET LPC is a transonic three-stage compressor. Experimental data will be available at measurement planes within the AIP as well as behind the LPC strut. Thus, the final calculation domain includes spinner nose and strut.

3.1 Mesh and Boundary Conditions

The LPC mesh was generated by the software NUMECA AutoGrid5 [12], using an O4H-topology. Cavities are not considered in order to reduce the number of cells. The radial distribution for total pressure, total temperature, and inflow angles at the inlet and a static pressure boundary condition at the outlet were modelled by a non-reflecting, one dimensional Fourier approach for both the steady and unsteady simulations.

3.2 Mesh Density Study

The standard mesh density based on MTU experience led to a mesh (called *Basic* further on) with about 8.9m cells for the seven blade rows of one LPC passage and a dimensionless wall distance $y^+ = 3$. Extended to a full annulus configuration, a not tolerable total cell number of 324m would arise for this mesh. Coarsened meshes (summarized in Tab. 1) were thus created with the condition to still be able to accurately simulate the stage matching.

Tab. 1. Cell numbers for mesh density study

Mesh	Cells [m] passage	Cells [m] 360°	Cell ratio 360°
Basic	8.91	324.76	1
Coarse1	1.26	46.28	0.142
Coarse2	1.62	57.21	0.176
Coarse3	3.42	93.16	0.287

Speed lines at the operation point of the future experiment were calculated for steady passage calculations with mixing planes. Therefore, the static outlet pressure was increased until numerical instability occurred. In this context, a convergence criterion of 0.005% was used for mass flow and pressure ratio and 0.02% for isentropic efficiency. The resulting compressor map is shown in Fig. 2, where no full speedline was calculated for *Coarse1*.

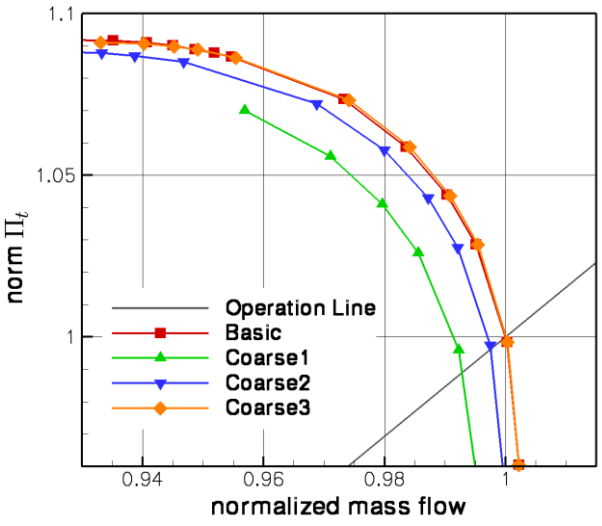

Fig. 2. Compressor map for different LPC meshes

3.2.1 Coarse1

After a coarsening of a modified *Basic* mesh by a factor 2 in every spatial direction, the first coarse mesh also features a $y^+ = 3$ at the blade surfaces as well as the hub and tip walls. This results in a reduction of cell number by more than 85%. The shape of the resulting speedline is similar to the reference line but the single operation points are shifted to reduced mass

flows (about 1%) and a slightly lower pressure ratio.

3.2.2 Coarse2

The next mesh is based on *Coarse1* but with a reduced y^+ of 1.5 on the blade surfaces. The resulting speedline moves closer towards the reference line. Following to subsequent investigations, the blade y^+-value directly influences the flow angle turning as well as the profile losses and thus pressure ratio and isentropic efficiency. As different flow effects cancel out each other for the present MexJET compressor geometry, a coarse mesh can lead to a rather good alignment with the reference speedline.

For a more detailed understanding of the effects of the mesh modification, the single stage and row characteristics were analyzed. The largest deviation in pressure ratio and turning angle between *Basic* and *Coarse2* was located within the rotor of the first stage.

3.2.3 Coarse 3

Therefore, the rotor 1 mesh of *Basic* was combined with the subsequent rows of *Coarse2*. At low throttle points, this line nearly perfectly aligns with the reference speed line. Extended to a full wheel configuration, a total mesh number of about 93m cells arose, which lies within the tolerable range.

3.3 Time-step study

An adequate calculation of the unsteady compressor flow field is also dependent on the temporal resolution of the URANS simulation. The increased computational effort compared to steady calculations is dependent on the number of time-steps per period as well as the number of sub-iterations per time-step. Thus, a reduction of temporal resolution directly leads to a decreased calculation time.

Unsteady simulations featuring zonal interfaces require an equal circumferential extent of the blade rows. The LPC configuration offers the possibility for a calculation of a 2π/10 (36°) segment through a domain scaling by a maximum of 2 blades (<5%) per row. This leads to comparable results while the computational effort is drastically reduced.

3.3.1 Time Step Size

The maximum frequency of an unsteady flow phenomenon that can be captured by an URANS-simulation is dependent on the used time-step size as well as the mesh cell size. Within a rotor-stator context, the rotating structures depend on the tangential frequencies which are related to the extent of the smallest cell in circumferential direction. Following a method proposed by Gourdain and Leboeuf [13], the maximum frequency that can be resolved with the final mesh is about 37 times the blade passing frequency of the first rotor, BPF_{R1}. A reference number of 1440 time-steps per rotor revolution was thus taken to allow a temporal resolution of $f_{max} = 36 \cdot BPF_{R1}$ following the Nyquist-Shannon sampling theorem. The resulting number of 72 time steps per rotor 1 passage lies within the recommended range of 64 to 128 for TRACE [7]. Due to the higher number of blades in rotor 2 and 3, a reduced temporal resolution arises for these rows but a further increase in time step number was not feasible with the available computer resources. Compared to rig experiments, the validation data gained within the experiment will only deliver a limited degree of detail as already mentioned. Additionally, as shown within the mesh density study, rotor 1 plays the major role for the overall LPC performance and also has the highest influence on the duct distortion and vice versa.

TRACE solves the discretized URANS-equations via a dual-time-stepping approach. In order to increase numerical stability, the pseudo-time is locally adapted to the physical time step and hence depends on the time resolution and the number of sub-iterations in each time step. In case the pseudo-time step and physical time-step differ strongly, an adaption via the CFL number or time-resolution is recommended.

In the following study, a name convention is used to describe the specific setups. “720-20-200” relates to 720 time-steps per full rotor revolution, 20 sub-iterations per time-step and a CFL number of 200. The initial number of 1440 time-steps per revolution was subsequently reduced to 720, 360, and 180.

3.3.2 Convergence Control

The determination of convergence of an unsteady simulation includes both the convergence of the individual time-steps as well as a constant periodic state of the resulting flow field [14]. The residual of the discrete sub-iterations per time-step is shown for a temporal discretization of 720 time steps per revolution in Fig. 3.

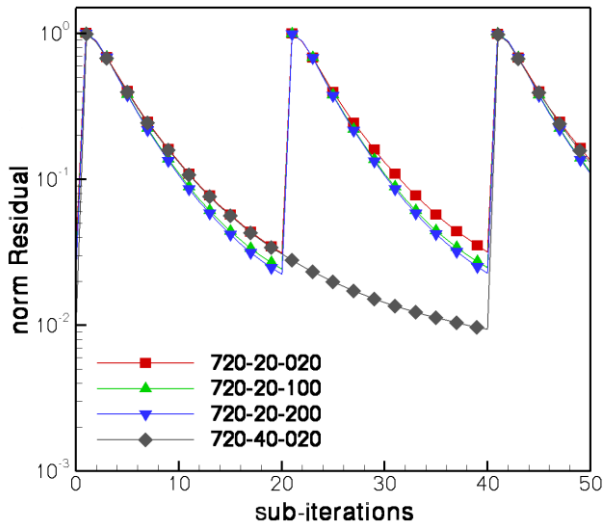

Fig. 3. Convergence of an unsteady time-step over sub-iterations

A number of 20 sub-iterations per time-step already leads to a residual drop of more than 1.5 orders of magnitude as recommended for this solver. This behavior was found to be independent on the time-step sizes used within the study. An increase in CFL number leads to a slightly faster residual drop.

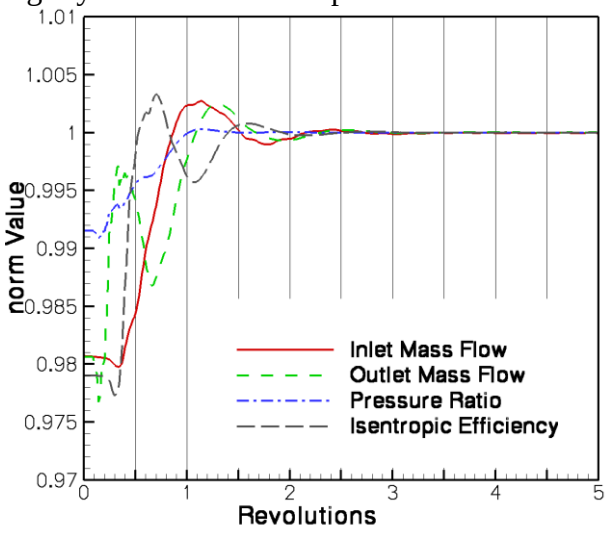

Fig. 4. Convergence of time-averaged parameters of an unsteady 36° simulation

An unsteady convergence of the global performance parameters mass flow, total pressure ratio, and isentropic efficiency averaged over one 36° period (cf. Fig. 4) was observed after 3-4 full rotor revolutions. The temporal oscillations of unsteady probe data such as velocities or pressure signals throughout the LPC also reveal periodic convergence. Processed by a Fast Fourier Transformation (FFT), amplitude and phase of several signals show convergence after 4 rotor revolutions.

3.3.3 Results

The global operation point within the compressor map of the 1440, 720, and 360 time-step setup are nearly identical, whereas the coarsest setup shows a slight increase in mass flow and pressure ratio. These differences are also visible in the radial distribution of total pressure ratio of the three stages normalized by the results of the 1440 time-step setup as shown in Fig. 5.

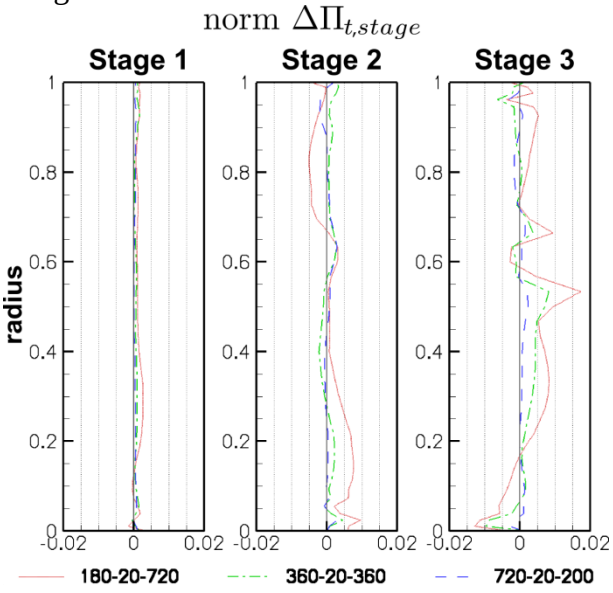

Fig. 5. Differences in radial distribution of stage total pressure ratio, normalized by the 1440-20-100 setup

The radial differences grow with increasing time-step size and stage number. On the one hand, the increasing number of blades within the rows of stage 2 and 3 leads to an additional reduction of time-steps per blade passage, on the other hand, the discrepancies add up throughout the LPC which was also described in a similar study by Schreiber et al. [14]. However, even for the 360 time-step setup, the local deviations stay below 1%.

A more detailed view on the rotor-stator interactions was obtained by an analysis of unsteady probe signals. Total pressure signals were chosen, as they show losses in rotor and stator wakes as well as upstream travelling pressure distortions generated by e.g. leading edge shock waves. The first probe is located within the rotating frame of reference, close to the leading edge of rotor 2 at 70% radial height. The signals, normalized by their temporal average in Fig. 6 indicate the wakes of stator 1 for nearly all time-step sizes.

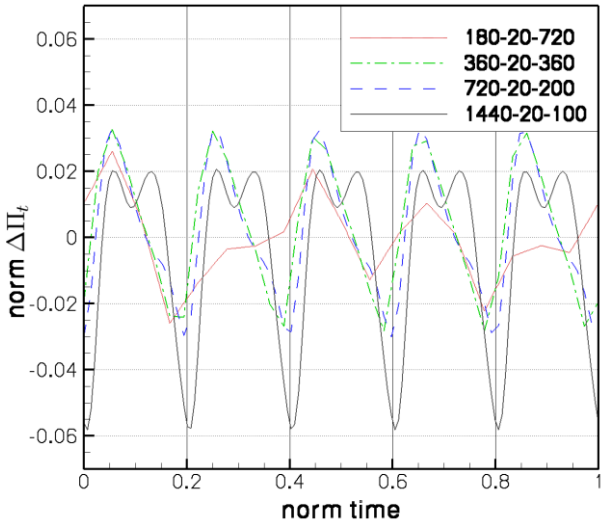

Fig. 6. Unsteady total pressure probe data at 70% radius at outlet of stator 1 (rotor frame)

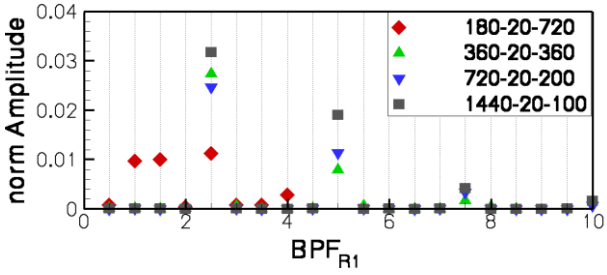

Fig. 7. FFT analysis of total pressure probe data at 70% radius at outlet of stator 1 (rotor frame)

Within the FFT data in Fig. 7 the basic frequency of stator 1, equal to 2.5 times the blade passing frequency of rotor 1 (BPF_{R1}) as well as its higher harmonics are clearly visible for the 360, 720 and 1440 setup with varying amplitude. The setup with 180 time-steps per revolution shows a poor representation of the signal as well as additional frequency peaks, which cannot be related to any blade passing phenomenon.

The signal of two rotor 1 wakes measured in the stator 1 frame at 30% radial height is presented in Fig. 8. For the higher time-step number, additional, superpositioned frequencies are visible.

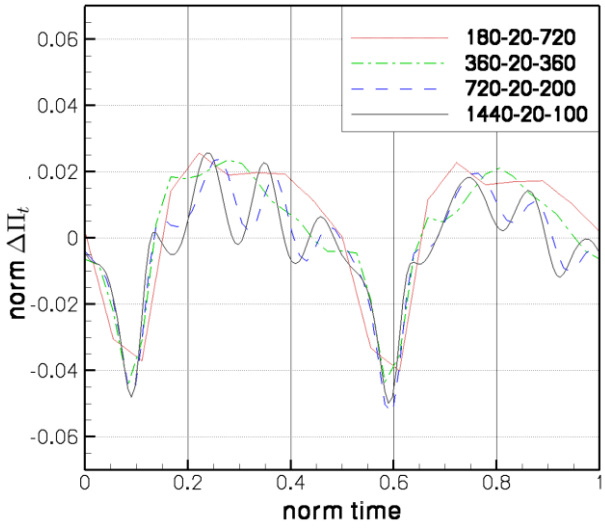

Fig. 8. Unsteady total pressure probe data at 30% radius at outlet of rotor 1(stator frame)

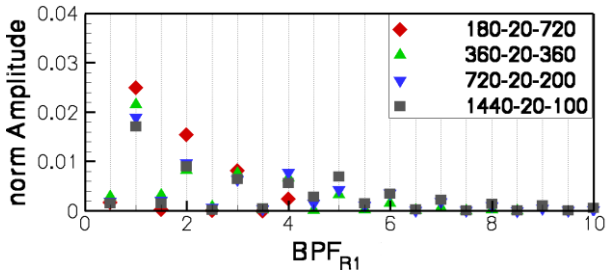

Fig. 9. FFT analysis of total pressure probe data at 30% radius at outlet of rotor 1 (stator frame)

The FFT data in Fig. 9 shows the peak for the rotor 1 BPF and its harmonics, but also a peak at 4.5 BPF_{R1} which is no integer multiple.

The FFT of the total pressure signal at the same axial position but at 70% (cf. Fig. 10) reveals even stronger amplitudes of these additional, non-harmonic frequencies.

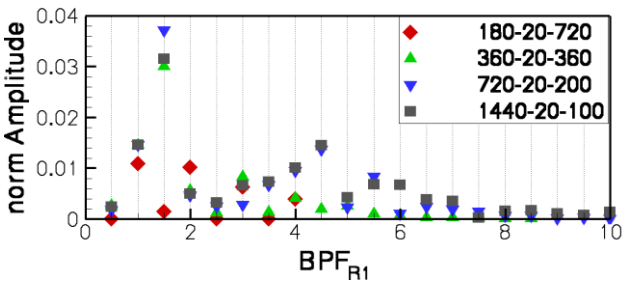

Fig. 10. FFT analysis total pressure of probe data at 70% radius at outlet of rotor 1 (stator frame)

Upstream travelling pressure distortions of the subsequent, transonic rotor rows are expected to be responsible for these additional peaks, which are not present within the probe signals of variables with a strong convective character such as eddy viscosity or turbulent kinetic energy. While the 360 setup showed a proper representation of the stator wakes in Fig. 6, it fails to capture these rotor interactions.

720 time-steps per revolution lead to a very good representation of the global and stage pressure ratios. Rotor-stator interactions are sufficiently captured while a reduction of computational effort by the factor 2 is achieved. Therefore this setup will be used for the coupled full annulus simulations.

3.3.4 Calculation Effort

The simulation duration in CPU hours per rotor revolution and million mesh cells for the presented simulations are summarized in Tab. 2.

Tab. 2. CPU resources for different time-step sizes

Setup	CPUh/rev/m	CPUh ratio
1440-20-100	64.04	1
720-20-200	33.95	0.53
360-20-360	17.49	0.27
180-20-720	8.93	0.14

In order to estimate the required CPU time for the full annulus configuration, as well as to validate the used convergence criteria, an isolated, undistorted 360° LPC simulation was carried out.

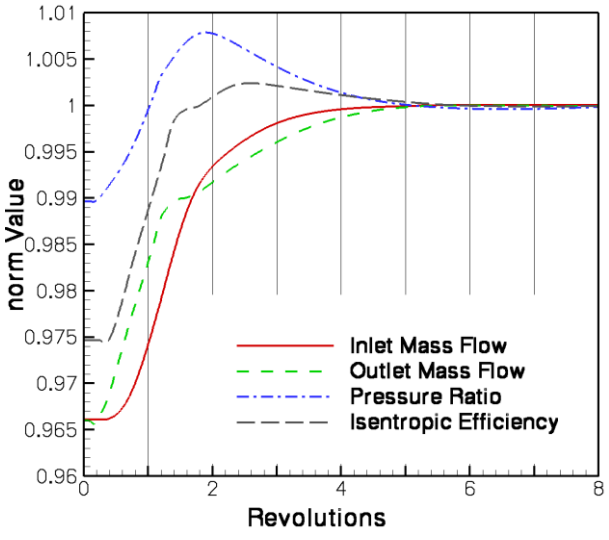

Fig. 11. Convergence of time-averaged performance parameters for full annulus configuration

The resulting global performance parameters (cf. Fig. 11), as well as unsteady probe data suggest an increased number of required revolutions for convergence compared to the 36° calculations. This increase in convergence time might also be influenced by a poorer initial solution (mass flows at 96.5 % of final value compared to 98% in Fig. 4).

The measured CPU hours per revolution and million cells rose to 162, corresponding to a calculation real time of 120 hours per rotor revolution on 128 cores. This means a loss of parallelization efficiency from 90% for the 36° calculations to about 59%. An update for solver and parallelization algorithm reduced the calculation time to 16h per revolution.

4 Isolated Intake Simulation

The bent intake geometry presented in Fig. 12 was developed to meet mechanical as well as aerodynamic requirements for the integration within the institute's Engine Test Facility (ETF) [5]. A strong AIP distortion leading to a significant interaction between compressor and duct was aimed for respecting the MexJET engine specification to assure a safe operation.

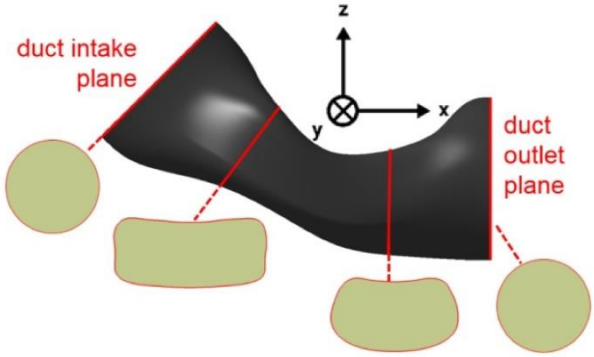

Fig. 12. Intake duct geometry [6]

TRACE was developed and calibrated as a turbo machinery solver. Hence, an extensive parameter study was performed within this context to find the ideal numerical setup for intake calculations [15]. Finally, the *k-ω* turbulence model in combination with an additional streamline curvature correction [16] showed the best performance and was applied for the duct domain both in isolated as well as coupled simulations.

4.1 Mesh and Boundary Conditions

This study led to a structured butterfly mesh with about 1.46m cells. Wall functions ($y^+ \approx 3$) were applied as no improvement was observed for the use of a Low Reynolds wall formulation.

Caused by the unconventional design of the ETF, non-uniform inflow conditions arise. Within the final experiment, these conditions will be measured by a traversable measurement rake. During the design phase of the duct, the boundary conditions were estimated by a numerical simulation of the ETF. Inlet and outlet domains are modelled by a two dimensional non-reflecting Riemann boundary condition.

4.2 Steady Intake Calculations

Steady calculations suggest a combined total pressure and swirl distortion towards the AIP as depicted in Fig. 13. The total pressure distortion in the upper half of the AIP lies within a separated flow regime with negative axial velocity. The large flow separation as well as convergence problems suggested an unsteady behavior of the duct flow field.

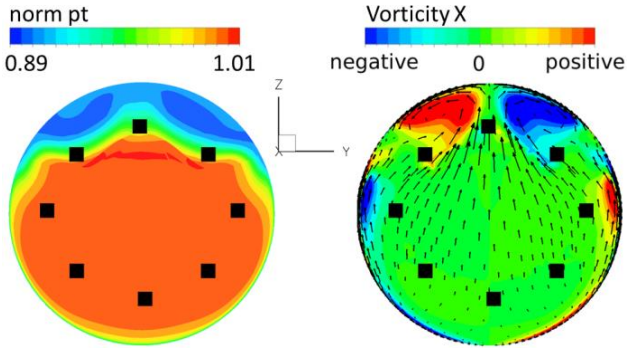

Fig. 13. AIP total pressure (left) and swirl (right) flow distortion for steady calculations and probe positions (black squares)

4.3 Unsteady Intake Calculations

The duct was then simulated in unsteady mode featuring the time-step sizes used within the LPC parameter study. Due to the low cell number of the intake domain, it was possible to simulate a time of 100 rotor revolutions.

All time-step sizes used in 3.3 show comparable results for the intake inlet and AIP mass flows in Fig. 14. In this plot, three periods can be separated: One of constant mass flow (0-30 rev), a region of low amplitude sinusoidal fluctuations (30-55) and finally rather random mass flow fluctuations with an amplitude of around 4% at the inlet and 2% within the AIP.

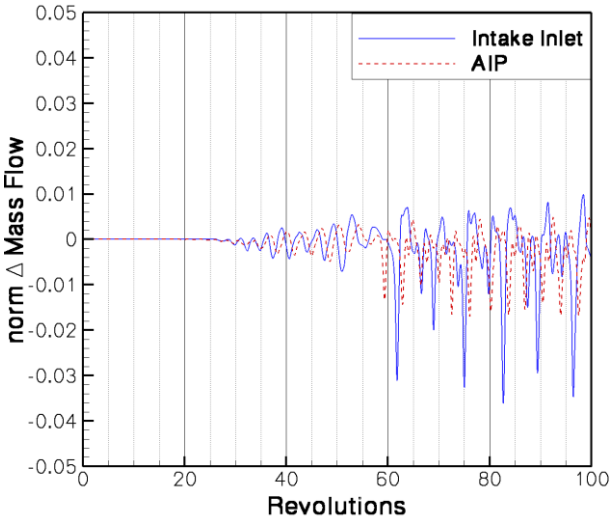

Fig. 14. Mass flow fluctuations for an isolated unsteady intake simulation

The unsteady character of the intake flow field is caused by the flow separation at the upper duct wall in the region with strong curvature close to the AIP. Among others, the wake of this flow separation leads to total pressure fluctuations at numerical probes, positioned on 8 circumferential AIP positions within at 70% radius presented in Fig. 15.

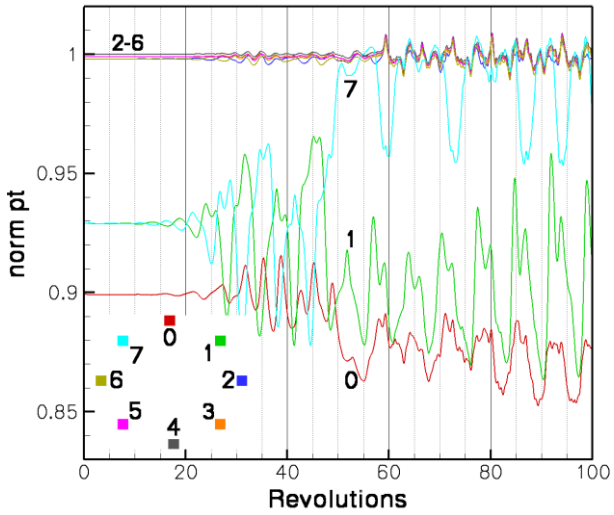

Fig. 15. Total pressure data of probes 0-7 at 70% radius within AIP for an isolated unsteady intake geometry

The strongest total pressure amplitudes of up to 10% were identified within the wake for probes 7, 0, and 1. The data also shows the three previously described periods whereas the

first total pressure fluctuations occur already after about 10 rotor revolutions. This "convergence time" must later be considered within the coupled simulations. Even after 100 revolutions, no constant amplitudes could be observed.

5 Coupled Simulation

For the coupled setup, the "butterfly" duct mesh topology was connected to the rotationally symmetric LPC mesh via an additional zonal interface within the AIP. The resulting mesh comprises about 101m cells, the calculation time added up to 0.41 CPU hours per revolution and million cells (roughly 2 days real time per revolution on 128 cores).

5.1 Convergence

Mass flow fluctuations of this simulation are summarized over nearly 50 revolutions in Fig. 16, where the onset of an oscillating behavior after 12-15 revolutions can be observed.

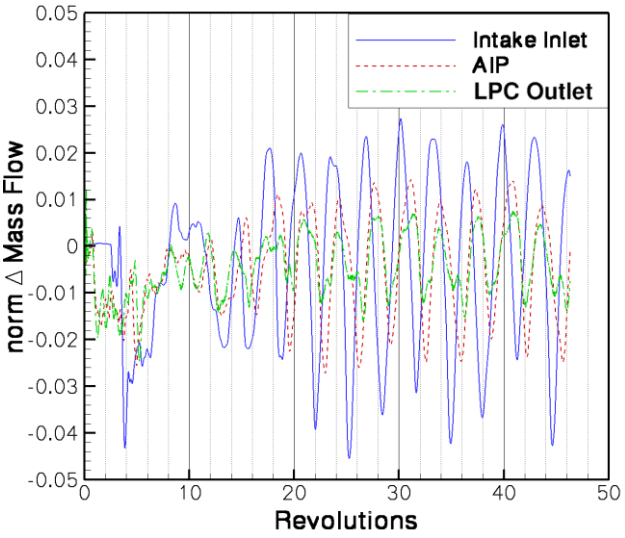

Fig. 16. Total pressure data of probes 0-7 at 70% radius within AIP for an isolated unsteady intake geometry

Compared to the isolated intake calculations, the mass flow fluctuations feature both an increased amplitude (about 4% at AIP) and frequency (about 3 revolutions) due to the interaction between intake and compressor. Similar to the isolated intake simulations, no converged unsteady state with constant amplitudes can be detected at this point. The same was observed for other parameters such as LPC pressure ratio or AIP total pressure fluctuations. The mechanisms responsible for this behavior are not yet fully understood and will be subject of further publications.

6 Conclusion and Outlook

Within this paper, steady and unsteady numerical simulations of an intake duct and a transonic three-stage low pressure compressor were carried out in preparation of a coupled simulation of both components. Purpose was the reduction of spatial and temporal resolution due to limited computational resources. The resulting losses in solution accuracy were quantified and traded versus the savings in calculation effort. The main conclusions can be summarized as follows:

- Rotor 1 plays a major role, both in overall compressor performance as well as intake-compressor interaction. A reduction of spatial and temporal resolution in the subsequent rows has a minor effect on the flow solution for the compressor under consideration here.
- Coarsening of the compressor mesh in combination with a reduction of blade surface cell height leads to a favorable cell number – precision ratio.
- The convergence of time-averaged global machine parameters such as mass flow, total pressure ratio, and isentropic efficiency implies the convergence of an unsteady periodic state.
- The reduction of the recommended number of time-steps per revolution by a factor of 2 leads to a tolerable loss of detail concerning compressor and stage pressure ratio as well as rotor-stator interactions.
- The low frequency unsteady flow regime within the intake is captured well by the high temporal resolution necessary for the LPC calculation.
- To account for the transient oscillation, a simulated time of at least 15 rotor revolutions is required for the coupled simulations.

The data gained by the later ETF experiments, will allow for a validation of numerical models especially for intake simulations as well as an

evaluation of the presented simplifications in spatial and temporal resolution. A deeper understanding of the interaction of intake flow and distorted compressor are expected from both, simulation and experiment.

Acknowledgements

These simulations were carried out within the scope of the COORETEC-Turbo 2020 project no. 1.2.4a. "Stabilität des Verdichtersystems bei Off-Design Zuströmbedingungen". This AG Turbo project is funded by the German Ministry of Economy and Technology (BMWi) and conducted in cooperation with MTU Aero Engines.

References

[1] Rademakers R.P.M, Bindl S and Niehuis R. "Influence of Secondary Flow within Integrated Engine Inlets on the Performance and Stability of a Jet Engine". *Proc of 22th ISABE Conference*, Phoenix, USA, ISABE-2015-20020, 2015.

[2] Brear M.J, Warfield Z and Mangus J F. Flow "Separation within the Engine Inlet of an Uninhabited Combat Air Vehicle (UCAV)". *Proc of FEDSM'03, 4th ASME Joint Fluids Engineering Conference*, Honolulu, USA, 2003.

[3] Society of Automotive Engineers, "Gas Turbine Engine Inlet Flow Distortion Guidelines". *Technical Report* 1420, Rev. B, 2011.

[4] Niehuis R, Lesser A, Probst A, Radespiel R, Schulze S, Kähler C.J, Spiering F, Kroll N, Warzeck F and Schiffer H.P. "Simulation of Nacelle Stall and Engine Response". *Proc of 21st ISABE Conference*, Busan, South Korea, ISABE-2013-1308, 2013.

[5] Gunn E.J. and Hall C.A. "Aerodynamics of Boundary Layer Ingesting Fans". *Proc of ASME Turbo Expo 2014: Technical Conference and Exposition*, Düsseldorf, Gerrmany, GT2014-26142, 2014.

[6] Rademakers R.P.M, Kächele T and Niehuis R. "Integration of a Highly Bent Engine Inlet in an Engine Test Facility". *Proc of ISROMAC Symposium of Rotating Machinery*, Honolulu, USA, ISROMAC2016-112, 2016.

[7] Nürnberger D. „Implizite Zeitintegration für die Simulation von Turbomaschinenströmungen". *Dissertation. DLR Forschungsbericht 2004-27*, 2004.

[8] Kügeler E. „Numerisches Verfahren zur genauen Analyse der Kühleffektivität filmgekühlter Turbinenschaufeln". *Dissertation. DLR-Forschungsbericht 2005-11*, 2005.

[9] Lesser A. and Niehuis R. "Transonic Axial Compressors with Total Pressure Inlet Flow Field Distortion". *Proc of ASME Turbo Expo 2014: Technical Conference and Exposition*, Düsseldorf, Gerrmany, GT2014-26627, 2014.

[10] Schoenweitz D. and Schnell R. „Development and Evaluation of a Performance Estimation Methodology for Fans Operating Within Non-Homogenous Inflow".*Proc of ASME Turbo Expo 2016: Technical Conference and Exposition*, Seoul, South Korea, GT2016-57095, 2016.

[11] Kozulovic D, Röber T, Kügeler D and Nürnberger D. "Modification of a Two-equation Turbulence Model for Turbumachinery Fluid Flows". *Deutscher Luft- und Raumfahrtkongress*, Dresden, Germany, DGLR-2004-229a, 2004.

[12] User Manual - Automated Grid Generator for Turbomachinery. *NUMECA International*, Brussels, Belgium, 2014

[13] Gourdain N and Leboeuf F. "Unsteady Simulation of an Axial Compressor Stage With Casing and Blade Passive Treatments", *J. Turbomach.*, vol. 131, no. 2, p. 021013, 2009

[14] Schreiber J, Ottavy X, Ngo Boum G, Aubert S and Sicot F. "Numerical Simulation of the Flow Field in a High Speed Multistage Compressor – Study of the Time Discretization Sensitivity". *Proc of ASME Turbo Expo 2015: Turbine Technical Conference and Exposition*, Montreal, Canada, GT2015-42114, 2004.

[15] Kächele T, Schneider T, and Niehuis R. "Steady and Unsteady CFD Simulation of a Bent Intake Geometry". *20. DGLR-Fach-Symposium der STAB*, Braunschweig, Germany, Abstact currently under review, 2016.

[16] Kozulovic D and Röber T. "Modelling the Streamline Curvature Effects in Turbomachinery Flows". *Proc of ASME Turbo Expo 2006: Power for Land, Sea and Air*, Barcelona, Spain, GT2006-90265, 2006.

Copyright Statement